

WATER-ICE, WATER VAPOR AND DUST AT THE PHOENIX LANDING LATITUDES AND SEASONS.

L. K. Tamppari¹, M. D. Smith², D. S. Bass¹, and A. S. Hale¹. ¹Jet Propulsion Laboratory/Caltech, 4300 Oak Grove Dr., M/S 264-623, Pasadena, CA 91109, ²NASA Goddard Space Flight Center, Mail Code 693, Greenbelt, MD 20771.

Introduction: The Phoenix Mars Scout mission is planning to carry two experiments that will observe water-ice, water-vapor, and dust in the Martian atmosphere: a solid state imager, developed by the University of Arizona, and an upward-looking lidar, contributed by the Canadian Space Agency. Because of this capability, observations of these quantities from previous spacecraft are important as background information and context for this mission. In particular, spring and summer observations of the north polar region are relevant as Phoenix will launch in August 2007 and land in the north polar region between 65-72N near $L_s=80$. The Phoenix engineering team is also interested in water-ice and dust opacities as both water-ice and dust optical depth will affect the amount of sunlight impinging upon the solar panels, thus modifying the amount of solar energy present to power the spacecraft and instruments. Dust in the atmosphere will affect the surface and near-surface atmosphere temperatures, which in turn could affect the amount of heater power needed to keep the spacecraft warm (it is passively cooled). Finally, the spacecraft entry, descent and landing will be affected by the amount of dust present due to its affect on the atmospheric temperature profile and therefore the density profile that the spacecraft experiences.

Data Sets: The water vapor and water-ice and dust optical depth mapping shown here utilizes the data from the MGS TES instrument. It is an infrared interferometer/spectrometer operating in the spectral range 6-50 μm [1]. In particular, the water-ice clouds are retrieved using the ~12-mm (825 cm^{-1}) water-ice absorption feature and the dust is retrieved using the ~9-mm (1075 cm^{-1}) [2,3]. Water vapor is retrieved using 5 bands spanning 28-42 μm .

The MGS spacecraft is in a sun-synchronous, nearly polar orbit [1]. The spacecraft orbits Mars 12 times every 1-sol period covering the globe with equally spaced strips once a day. The data are taken around the local time of 1400 hours and 0200 hours. Here, we use the daytime (~1400 hour) data. At this time of day, water-ice cloud formation is likely to be near the minimum since the diurnal temperatures will be near the maximum [e.g., 4]. As such, water-ice optical depths noted here are likely a lower limit on the amount present over the diurnal cycle.

Mapping of atmospheric quantities: The atmospheric quantities mapped here, using MGS TES observations, span nearly three Mars spring/summer

seasons, from $L_s \approx 104$ in Mars year 24 (1999-2000) to $L_s \approx 180$ in Mars year 26 (2002-2003; Mars years definitions per [5]). L_s is defined as the areocentric longitude of the sun, with $L_s=0$ starting at northern spring equinox and stepping through the seasons to $L_s=359$, just before the subsequent northern spring equinox. The data examined cover 60-90°N latitude during the Mars northern spring and summer times ($L_s=0-180$). Because of the low surface temperature in these northern latitudes, which decreases the signal to noise, the data examined here are retrieved only over a surface of $T > 220\text{K}$.

To produce seasonal maps, we average the optical depths and the vapor in boxes of 2° latitude by 4° longitude by 5° in L_s (Figures 1 and 2 for water-ice and dust, respectively and Figure 3 for water vapor). We chose this combination of parameters to maximize the areal coverage while minimizing the time step from map to map, and to allow averaging of many retrievals together, minimizing the uncertainties in each bin. The mathematical mean is computed for each bin using the total number of points that fell into that lat/lon/ L_s bin. The typical number of points in any one bin is 10-20, and so we assume that the uncertainties in each bin are 0.025 or 5% of the optical depth. The color scale for the maps shows absorption-only optical depths for $\tau_{12\mu\text{m}}$ (water-ice) on a scale of 0-0.2 and $\tau_{9\mu\text{m}}$ (dust) on a scale of 0-0.4. For water vapor, the color scale ranges from 0-100 pr μm . The dynamic range of each of the scale bars was chosen to “stretch” the signal and bring out variations within the maps. In actuality, the largest value in a given map is often larger than the maximum shown and, in those cases, is colored to the maximum color on the scale bar. The black area in the maps contains no data. The black area surrounding the northpole is due to surface temperature cutoff of $T_s > 220\text{K}$. This area decreases and subsequently increases, following the retreat and growth of the seasonal polar cap.

Maps for all years and seasons will be shown and discussed at the conference.

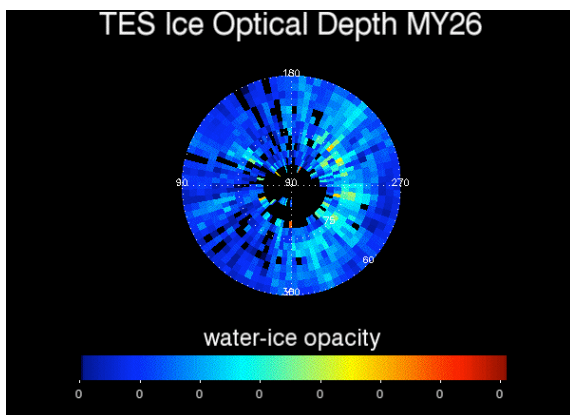


Figure 1. TES infrared (12-micron) water-ice optical depth map for MY26, $L_s=95-110$. The color scale bar ranges from 0-0.2.

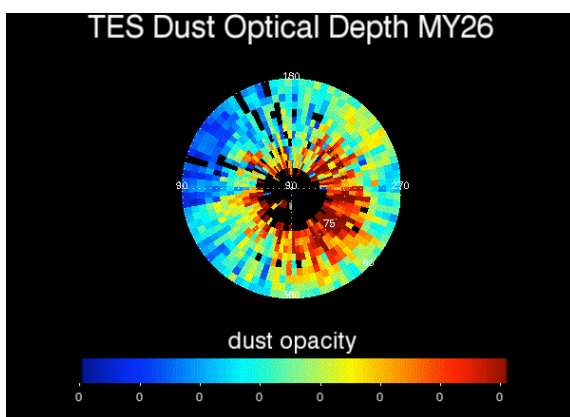


Figure 2. TES infrared (9-micron) dust optical depth map for MY26, $L_s=95-110$. The color scale bar ranges from 0-0.4.

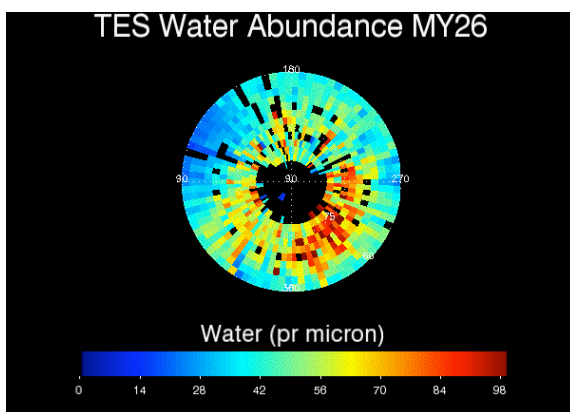


Figure 3. TES water vapor map for MY26, $L_s=95-110$. The color bar ranges from 0=100 pr μm .

Conclusions:

The water-ice cloud and dust optical depths and water vapor have been mapped in the north polar region during northern spring and summer for three Mars Years, beginning $L_s=105$ in MY24 (Mars Year

definitions per Clancy et al., 2000), using the Mars Global Surveyor Thermal Emission Spectrometer [6]. The observations discussed here are consistent with past work on clouds and dust using other techniques [e.g., 7, 3, 8]. Specific conclusions are:

1) Longitudinal variability in the optical thickness of the north polar hood (NPH) exists, both during springtime recession and late-summer onset. This variability varies interannually.

2) Each year, the breakdown of the seasonal NPH occurs about $L_s=70$ and the NPH reforms near about $L_s=160-165$.

3) Water-ice cloud background opacity levels decrease to summertime low levels (typically <0.1) starting at $L_s=80$ in each year. The opacities begin to rise again at different times in different years: $L_s=140$ for MY 24, $L_s=135$ for MY 25, and $L_s=110$ for MY 26.

4) The background water-ice opacities appear to reach minimum values in the longitudinal region 0-90 W between $L_s=105$ and $L_s=125$ in all years.

5) There is significant interannual variability in dust magnitude, but both MY 25 and 26 show peak dust (high magnitude over wide area) between $L_s=75-100$.

6) The longitudinal quadrant 0-90 W exhibits much higher dust opacities than other locations for many seasons in all years examined, but the details vary interannually. Both MY25 and 26 showed this region having the most dust between $L_s=65-85$.

7) There is evidence for stationary wavenumber 2 systems in the late spring in MY 26, characterized by elevated dust and water-ice in two opposite quadrants and reduced dust and water-ice in between.

8) Water vapor varies significantly interannually and varies spatially within a season.

9) Water vapor first increases above 50 pr μm near $L_s=75$ and decreases below 50 pr μm again near $L_s=130-125$. In between times, there are many locations in which the column abundance is >50 pr μm , even approaching 200 pr μm . This increase/decrease pattern is repeatable year to year.

Because these observations show the spatial and seasonal changes in atmospheric quantities over 3 Mars years, they will provide a useful background for Phoenix measurements and guide observational planning. The Phoenix mission will be 90 sols long, occurring between $L_s \approx 76-125$.

References: [1] Christensen, P. R., et al., *JGR* **97**, 1992. [2] Pearl et al., *JGR* **106**(E6), 2001. [3] Smith, M.D., *Icarus* **167**, 2004. [4] Pathak et al., submitted to *Icarus*, 2004. [5] Clancy, R. T., et al. *JGR* **105**, 2000. [6] Tamppari, L. K., et al., submitted to *Plan. and Sp. Sci.*, 2005. [7] Wang HQ, Ingersoll AP, *JGR* **107**(E10), 2002. [8] Cantor, B., et al., *JGR* **106**(E10),